



HAL
open science

Low and high resolution gamma-ray spectroscopy for the characterization of uranium contamination

F Salvador, T Marchais, B Perot, P.-G Allinei, F Morales, O Gueton, J Venara, M Cuzzo, P Fichet, F Mayet

► To cite this version:

F Salvador, T Marchais, B Perot, P.-G Allinei, F Morales, et al.. Low and high resolution gamma-ray spectroscopy for the characterization of uranium contamination. Nucl.Instrum.Meth.A, 2024, 1065, pp.169549. 10.1016/j.nima.2024.169549 . hal-04638936

HAL Id: hal-04638936

<https://hal.science/hal-04638936>

Submitted on 19 Jul 2024

HAL is a multi-disciplinary open access archive for the deposit and dissemination of scientific research documents, whether they are published or not. The documents may come from teaching and research institutions in France or abroad, or from public or private research centers.

L'archive ouverte pluridisciplinaire **HAL**, est destinée au dépôt et à la diffusion de documents scientifiques de niveau recherche, publiés ou non, émanant des établissements d'enseignement et de recherche français ou étrangers, des laboratoires publics ou privés.

1 Low and high-resolution gamma-ray spectroscopy for the 2 characterization of uranium contamination

3 F. Salvador ^a, T. Marchais ^{a,*}, B. Perot ^a, P-G. Alliney ^a, F. Morales ^a, O. Gueton ^b, J. Venara ^c,
4 M. Cuzzo ^c, P. Fichet ^d, F. Mayet ^e

5 ^aCEA, DES, IRESNE Institute, DTN, SMTA, Nuclear Measurement Laboratory, F-13108, Saint-Paul-Lez-
6 Durance, France

7 ^bCEA, DES, IRESNE Institute, Nuclear Technology Department, F-13108, Saint-Paul-Lez-Durance,
8 France

9 ^cCEA, DES, ISEC, DPME, SEIP, LNPA, Univ. Montpellier, Marcoule, F-30207, Bagnols-sur-Cèze, France

10 ^dCEA, DES, DDS, DFDE, SGOF, F-91191, Gif-sur-Yvette, France

11 ^eUniv. Grenoble Alpes, CNRS, LPSC-IN2P3, 53, avenue des Martyrs, 38000 Grenoble, France

12 *Corresponding author: Francisco.SALVADORBARBA@cea.fr (F. Salvador)

13 Keywords

14 In situ gamma-ray spectroscopy, NaI(Tl), HPGe, Uranium contamination, MCNP simulation,
15 Decommissioning nuclear facilities

16 Abstract

17 Decommissioning is the last step in the life cycle of a nuclear facility. After the evacuation of the facility
18 components, the remaining structures such as concrete walls and floors must be controlled to ensure
19 that no residual contamination remains. As it is a costly and time consuming activity, CEA develops fast
20 measurement methods allowing a complete scanning of very large areas (hundreds of thousands of
21 square meters) in legacy uranium enrichment plants based on gas diffusion, at Pierrelatte nuclear site,
22 France. After fast alpha and beta measurements, HPGe and NaI gamma-spectroscopy detectors are
23 used to characterize more precisely uranium contamination. HPGe has excellent energy resolution but
24 requires very long acquisition times. On the contrary, NaI(Tl) detectors enable rapid measurement, but
25 extracting the contamination signal from the natural background is difficult due to their low resolution.
26 Using an innovative approach based on energy bands of the NaI spectra, contamination activity and
27 enrichment are consistent with that measured with HPGe but in only 15 min vs. 65 h, and with a
28 sufficiently low relative uncertainty of about 15 % and 20 %, respectively, on activity and enrichment.
29 Large area NaI(Tl) detectors will allow cost-effective scanning of the Gaseous Diffusion Plant (UDG)
30 nuclear site (hundreds of thousands of squared meters) within practical times, in complement to alpha
31 and beta contamination detectors.

32 1 Introduction

33 The gaseous diffusion plant UDG is a legacy uranium enrichment facility currently under
34 decommissioning at Pierrelatte nuclear site, in south-eastern France. After the evacuation of large
35 equipment, the main objective is now the detection of residual low-activity uranium contaminated
36 areas on the floors and walls of the facility, which represent a total area to be controlled in the order

1 of 700 000 m². This contamination comes, for instance, from leaks that occurred during the 40-year
 2 operation lifespan. As all surfaces need to be checked with a very low clearance threshold of
 3 0.4 Bq.cm⁻² (alpha activity), CEA is currently developing measurement methods that meet low
 4 detection limits and fast counting times, by combining fast alpha and beta counting to perform a first
 5 level detection, and low-resolution gamma spectrometry with NaI(Tl) scintillation detectors as a
 6 second-level confirmation. The latter exhibits a poorer energy resolution than reference high-purity
 7 germanium semi-conductors, making a fine analysis of each gamma ray impossible. Still, NaI(Tl) crystals
 8 can be manufactured in much larger size and at lower cost than HPGe ones, allowing much larger
 9 detection efficiency and measurement times of a few minutes instead of hours. In this paper we
 10 present innovative NaI(Tl) spectrum analysis methods to estimate both the surface activity of uranium
 11 contamination and the ²³⁵U enrichment. We compare the results with HPGe reference measurements.
 12 The primary detection of contamination and its subsequent characterization rely on the detection of
 13 gamma rays emitted at specific energies listed in Table 1 [1].

14

Table 1 : Main gamma emissions of uranium contamination [2].

Decay chain	Isotope	Gamma energy (keV)	Gamma intensity (%)
²³⁸ U	²³⁸ U	49.55 (6)	0.0697 (26)
	²³⁴ Th	63.30 (2) *	3.75 (8)
		92.6 **	4.3
		112.81 (5) *	0.215 (22)
	^{234m} Pa	766.361 (20)	0.323 (4)
1 001.026 (18) *		0.847 (8)	
²³⁵ U	²³⁵ U	143.767 (3) *	10.94 (6)
		163.356 (3) *	5.08 (3)
		185.720 (4) *	57.0 (3)
		205.316 (4) *	5.02 (3)
	²³¹ Th	25.64 (2)	13.9 (7)
		84.2140 (13)	6.70 (7)
²³⁴ U	²³⁴ U	53.20 (2) *	0.1253 (40)

* Gamma rays used in this work

† The gamma ray listed at 92.6 keV corresponds to the mean energy of the 92.4 and 92.8 keV ²³⁴Th gamma emissions, which cannot be resolved due to the energy resolution of our detectors. The 4.3 % intensity is the sum of their intensities.

15
16
17
18
19

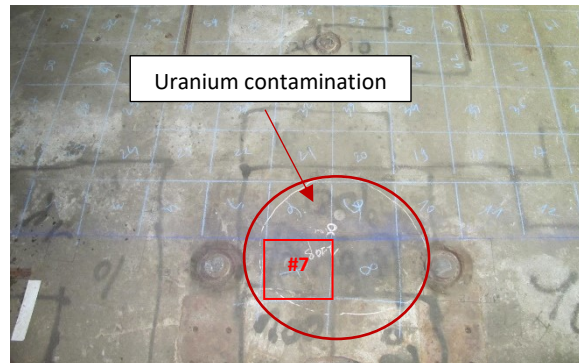
20 Natural gamma radiations from concrete soils and walls can be emitted at close energies of some peaks
 21 of interest, for instance the 186.2 gamma ray of ²²⁶Ra cannot be separated from that of ²³⁵U at 185.7
 22 keV, even with an HPGe detector. On the other hand, with a NaI(Tl) detector, radiations of the natural
 23 uranium and thorium chains, as well as that of ⁴⁰K, create a significant background made of broad
 24 peaks and a Compton continuum, which makes it difficult to detect a low-activity surface
 25 contamination. An exhaustive list of natural gamma emissions can be found in [1].

26

1 2 Measured areas and experimental setup

2 2.1 Measured area

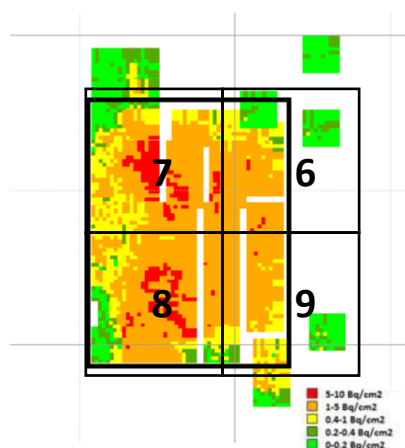
3 NaI(Tl) and HPGe measurements took place inside the UDG low-enrichment plant previously used to
4 produce uranium with a ^{235}U mass fraction between 0.35 % (depleted circuit) up to 2 % [3]. Both
5 detectors were placed successively in the same position, in the middle of square mesh #7 of Figure 1
6 (see also further Figure 2), which is a reference contaminated surface used to compare different
7 measurement techniques. This area was already characterized in our previous work reported in [1].



8
9 *Figure 1 : Measurement area containing a uranium contamination spot.*

10 It is important to mention that contamination in this area is highly heterogeneous, as shown in the
11 map of Figure 2 measured by numerical autoradiography using the Digital A Utoradiography
12 Measurement (MAUD), a 25 cm² detection surface alpha/beta camera developed by CEA based on
13 solid scintillators coupled to an array of 64 Silicon PhotoMultipliers (SiPM). With these characteristics
14 the camera is capable of achieving an image resolution of about 35 mm² [4] [5]. The map below stresses
15 the importance of a fine positioning of detectors over the spot of interest, in view to perform
16 quantitative comparisons. All measurements reported in this paper are performed with detectors in
17 the middle of mesh #7.

18



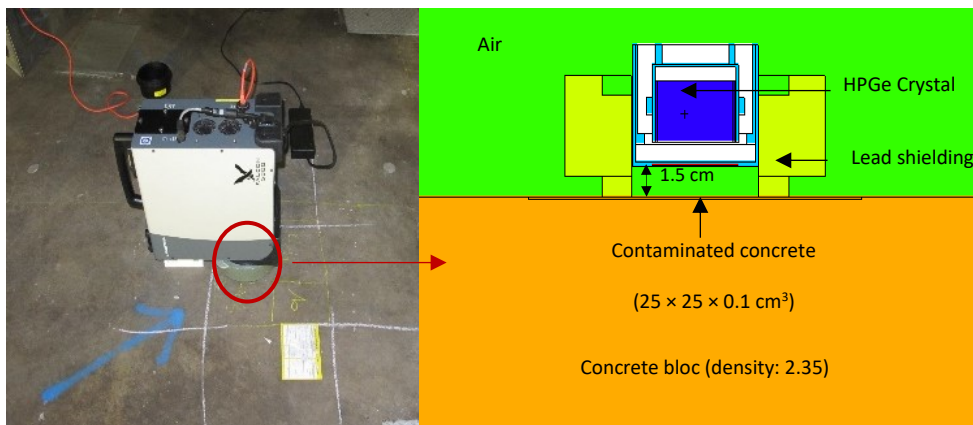
19

20 *Figure 2 : Fine activity mapping of the contaminated area measured with the Digital A Utoradiography Measurement*
21 *(MAUD) alpha/beta camera [4].*

1 Natural background acquisitions with the NaI(Tl) detector were also carried out in non-contaminated
2 areas of the low-enrichment, high-enrichment and very-high-enrichment plants. These measurements,
3 reported in section 4.2, are used to estimate the natural background and subtract it from the gross
4 count rate to obtain the net signal of the contamination.

5 2.2 Experimental setups and measured spectra

6 For high-resolution gamma spectroscopy acquisitions, we used an integrated Falcon 5000
7 spectrometer with a 6.5 cm diameter and 3 cm thick planar germanium crystal cooled with an electric
8 Peltier module, a digital electronics and a multi-channel analyzer [6]. During the acquisitions, the
9 detector was 1.5 cm above the floor and the crystal was surrounded by a 9.5 cm diameter lead ring to
10 limit the background noise from neighboring contaminated areas and from the natural background of
11 the walls. For low-resolution gamma spectrometry, we use a 4"×4"×2" NaI(Tl) detector (i.e. an area of
12 $10.2 \times 10.2 \text{ cm}^2$ and a thickness of 5.1 cm) in contact with the floor and surrounded by lead bricks. The
13 HPGe relative efficiency is about 18 % (with respect to the efficiency of a 3"×3" NaI scintillator for a
14 ^{60}Co source at 30 cm and at 1.332 keV, which worth about 10^{-3} [7]) and its energy resolution is 0.1 %
15 for the 1332 keV ^{60}Co peak (FWHM of about 1.3 keV). Comparatively, the NaI(Tl) detector shows a
16 resolution of 5 % at the same energy, and an efficiency even larger than that of a 3"×3" NaI(Tl) crystal.
17 Figure 3 and Figure 4 show the HPGe and NaI(Tl) experimental setups, as well as their Monte Carlo
18 simulation models developed with the Monte Carlo N-Particle (MCNP) computer code [8]. These
19 models are used to calculate the detection efficiencies of gamma rays stemming from the surface
20 contamination or from the underlying soil concrete, in case of the natural gamma-ray background. The
21 contaminated area in both simulation models was $25 \times 25 \text{ cm}^2$ as in [1], according to the grid of Figure
22 1. The thickness of 0.1 cm is based on a contamination depth estimation not reported in this work,
23 combining the alpha, beta and gamma measurements mentioned in introduction, as well as a multiple
24 peak analysis in high-resolution gamma spectroscopy.



25

26

Figure 3 : HPGe experimental setup and its MCNP model used for detection efficiency calculations.

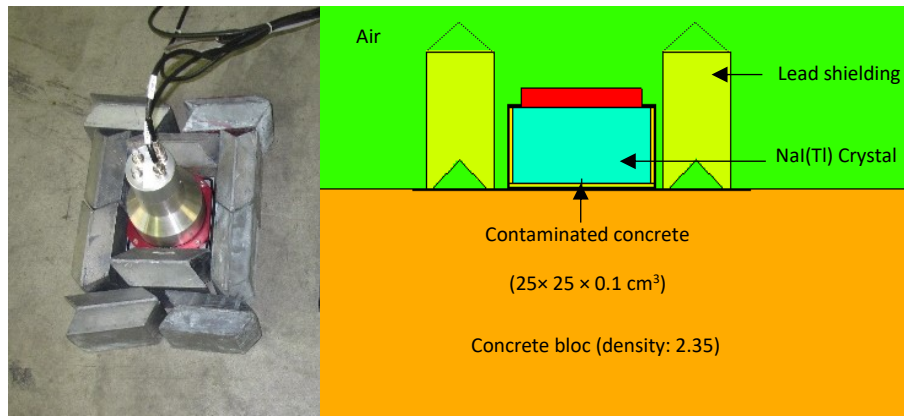


Figure 4 : NaI(Tl) experimental setup and its MCNP model used for detection efficiency calculations.

Based on the experimental configurations described above, we carried out a 65 h HPGe measurement and a 15 min NaI(Tl) measurement of the contaminated area, see spectra in Figure 5.

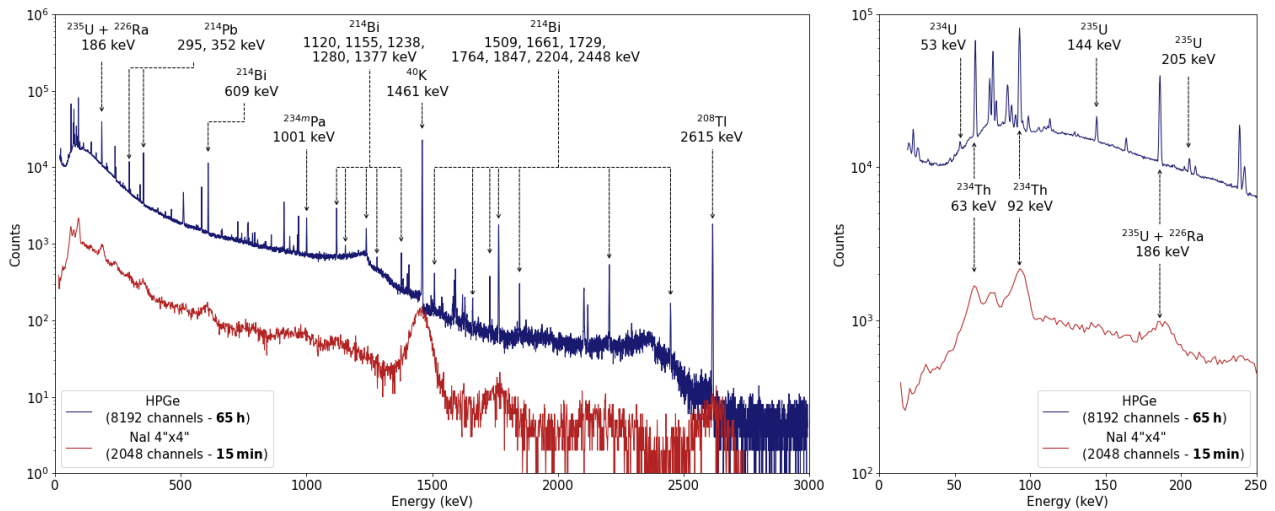


Figure 5 : Measured uranium contamination spectra after acquisitions of 65 h and 15 min with the HPGe and NaI(Tl) detectors, respectively.

The HPGe spectrum in Figure 5 shows gamma rays that are characteristic of the contamination, for example ^{238}U peaks at 63.3 keV, 92 keV (unresolved 92.4 keV and 92.8 keV gamma rays) and 1001 keV, ^{235}U peaks at 144 keV, 163 keV, 186 keV and 205 keV, and the 53.2 keV peak of ^{234}U . The cluster of peaks between 70 keV and 90 keV is due to X-rays spontaneously emitted in the soil concrete during the radioactive decays in the natural uranium and thorium chains (rearrangement after the ejection of internal conversion electrons), as well as fluorescence X-rays of the lead shielding.

The NaI(Tl) spectrum clearly shows that the analysis of individual peaks is not viable in most cases because of the scintillator lower energy resolution. Extracting net areas remains only possible for a few intense peaks, such as 63.3 keV, 92 keV and 186 keV, taking also into account possible interferences due to close neighboring gamma peaks like that of ^{226}Ra at 186 keV. In next sections, we present the reference results of the HPGe measurement and a comparison with these few net areas that can be extracted from the NaI(Tl) spectrum, then with an innovative method based on energy bands.

3 Characterization of the contamination with the HPGe detector

The main goal of the HPGe measurement is to provide reference values in terms of surface activity and enrichment of the contamination.

The surface activity is estimated as follows:

$$A_S(E) = \frac{S_N(E)}{Eff(E) \times I(E) \times T_c \times S_{contamination}} \quad (1)$$

with

- A_S the calculated surface activity (in Bq.cm⁻²) calculated with peak of energy E,
- $S_N(E)$ the net area under the gamma peak after subtraction of the Compton continuum under the peak,
- $Eff(E)$ the simulated detection efficiency (counts per source particle at energy E), calculated with the model presented in Figure 3, considering a uniform uranium contamination in the depth of 1 mm. Note that other depths ranging from a few μm to a few mm were also studied, showing a limited effect on gamma efficiency with a maximum relative difference of 4% at very low energy (53.2 keV),
- $I(E)$ the emission intensity at energy E (fractional number of gamma rays emitted per disintegration), from LARAWEB database [2],
- T_c the active counting time (in seconds),
- $S_{contamination}$ the area of the contamination (in cm²) taken into account in the MCNP model, here 25 × 25 = 625 cm² (see Figure 3).

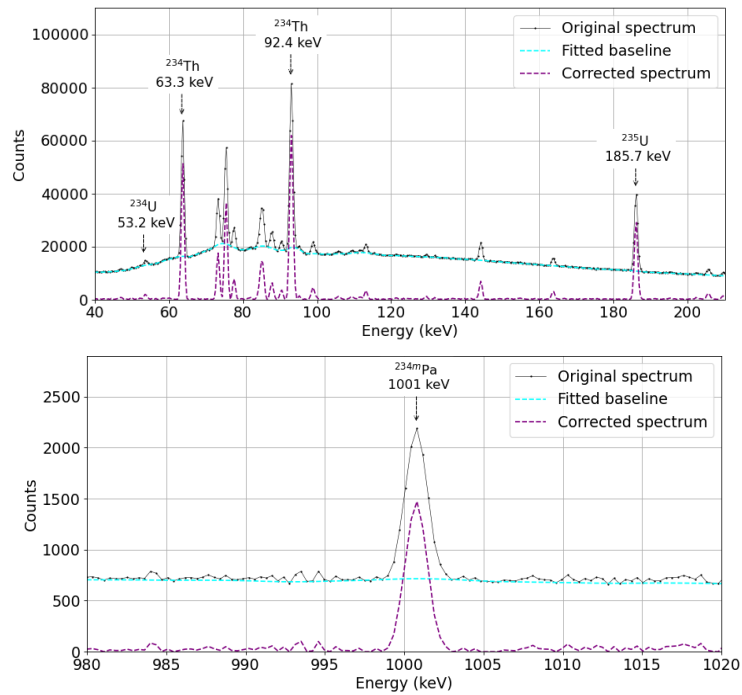
Using this formula, we are able to calculate a weighted-average activity for the ²³⁸U and ²³⁵U isotopes (which emit several detectable gamma rays, allowing each an activity estimation).

The ²³⁵U mass fraction, i.e. the uranium enrichment η_U , is calculated as follows:

$$\eta_U = \frac{m_{235}}{m_{235} + m_{238}} \times 100 \quad (2)$$

with m_{235} and m_{238} the ²³⁵U and ²³⁸U masses deduced from the respective ²³⁵U and ²³⁸U activities and their specific activities (in Bq.g⁻¹) extracted from [2]. Note that even if the alpha activity of ²³⁴U is due to its high specific activity, its mass fraction is much smaller than that of ²³⁵U and it can be neglected in (2).

Note that the calculation of net areas for (1) uses “pybaselines” [9], an automatic python script to subtract the Compton background with an “averaging morphological and mollified baseline” algorithm. Figure 6 shows the original HPGe spectrum and the corrected spectrum after subtraction of the Compton background.



1

2 *Figure 6 : Net area extraction in the HPGe spectrum, with a focus on the regions of interest [55 ; 210] and [980 ; 1020] keV*
 3 *containing the main gamma peaks listed in Table 1.*

4 It is important to note that due to a lack of time, the natural background of concrete could not be
 5 measured with the HPGe detector. Nonetheless, we can estimate the net background contribution
 6 inside the peaks of interest for contamination assessment, at 63.3, 92.4 & 92.8, 185.7 and 1001 keV,
 7 to respectively 3 %, 4 %, 7 % and 9 %. For this estimation, we calculate the activity concentration of
 8 natural ^{238}U in concrete (in $\text{Bq}\cdot\text{cm}^{-3}$) using several peaks of ^{214}Pb and ^{214}Bi (from the ^{238}U decay chain in
 9 secular equilibrium) and their detection efficiencies for gamma rays emitted in concrete, calculated
 10 with MCNP. Then, we calculate a weighted-average of the ^{238}U activity concentration, estimated with
 11 these different peaks, from which we can also deduce the activity concentration of ^{235}U in concrete,
 12 using the 99.3 % and 0.720 % natural abundances of ^{238}U and ^{235}U , respectively [10]. Finally, we can
 13 estimate the nets counts due to concrete background in the peaks of interest taking into account these
 14 uranium activities, the intensities of gamma rays given in Table 1 and their MCNP-simulated detection
 15 efficiency. Regarding the 185.7 keV peak of ^{235}U , we not only subtract the ^{235}U contribution of concrete,
 16 but also that of ^{226}Ra (^{238}U chain) at 186.2 keV, with its 3.56 % intensity. The total subtracted
 17 contribution is thus 7 %, which is similar to the fraction subtracted in this peak in our previous work
 18 [1], in which a HPGe concrete background measurement showed a contribution of about 9 % to the
 19 net area at 186 keV of the contamination spectrum. This small difference (7 % vs. 9 %) is probably due
 20 to the heterogeneity of surface contamination (see further Fig. 6), as we did not measure exactly the
 21 same spot inside mesh #7.

22 The surface activities reported in Table 2 are obtained after subtracting the background noise.

23

1 Table 2 : Activities of uranium isotopes in the surface contamination measured with the HPGe detector in a 65 h acquisition

Emitter isotope	Energy (keV)	Surface activity (Bq.cm ⁻²)	Mean activity (Bq.cm ⁻²)	Contribution to total activity (%)
²³⁸ U	63.3	2.91 ± 0.33	3.33 ± 0.33	44.5
	92.4 + 92.8	3.64 ± 0.47		
	1001	3.42 ± 0.38		
²³⁵ U	144	0.17 ± 0.02	0.18 ± 0.02	2.40
	163	0.18 ± 0.02		
	186	0.17 ± 0.02		
	205	0.18 ± 0.02		
²³⁴ U	53	3.97 ± 0.46	3.97 ± 0.46	53.1

2 Summing these means, the total surface activity of uranium contamination is
 3 **$A_s = (7.47 \pm 0.75) \text{ Bq.cm}^{-2}$** with a 10 % relative uncertainty resulting from the causes listed below.

4 We can also deduce the uranium enrichment of the contamination, $\eta_U = (0.83 \pm 0.07) \%$ using (2) and
 5 the mean activities of ²³⁸U and ²³⁵U from Table 2. This result is in the range of the expected values for
 6 the low-enrichment plant, *i.e.* from 0.35 to 2 % [3].

7 The error budget on activities is:

- 8 - uncertainties on gamma intensity, estimated to be below 6 % [2],
- 9 - relative statistical uncertainties on net area counts, which are globally less than 1 % thanks to
 10 the long measurement time, except for the low-intensity peak of ²³⁴U at 53.2 keV, for which it is
 11 12 %,
- 12 - the variability of the net area extractions depending on the fit parameters such as the number
 13 of channels on the left and right sides of the full energy peak, estimated to be below 1 %,
- 14 - the uncertainty on the simulated density and material composition of concrete, estimated to be
 15 5 % by simulating different concrete densities and compositions,
- 16 - the uncertainty on the detector numerical model, estimated to be 5 % by comparing
 17 experimental and simulation results obtained with standard ²⁴¹Am, ¹³⁷Cs, ⁶⁰Co, ¹⁵²Eu and ⁸⁸Y
 18 sources.

19 These results are quite different from our previous measurement, with a total surface activity reported
 20 in [1] of $A_s = 16.6 \pm 6.0 \text{ Bq.cm}^{-2}$ (while it is $A_s = 7.47 \pm 0.75 \text{ Bq.cm}^{-2}$ here). The former was measured
 21 with the HPGe a bit further from the ground (see Figure 5 of [1]), but most importantly, in a slightly
 22 different position inside the contaminated area. This last reason certainly explains the difference, as
 23 contamination is extremely heterogeneous, as shown above in Figure 2. Note that in the NaI(Tl)
 24 measurement described in next section, we have precisely positioned the detector in the same
 25 position as the HPGe detector to enable a more precise activity comparison. In addition, we plan to
 26 implement larger detectors in the future (typically 30 × 30 cm² scintillators) to reduce the sensitivity
 27 to heterogeneities.

28 In contrast, both measured uranium enrichments are similar, with $\eta_U = (0.83 \pm 0.07)\%$ here and
 29 $\eta_U = (0.80 \pm 0.13)\%$ in [1]. This is consistent with the fairly uniform enrichment in a same group of the
 30 facility.

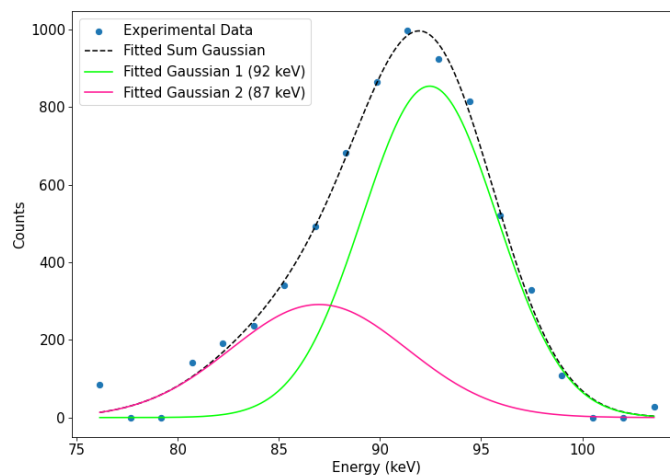
31

4 Characterization of the contamination with the NaI(Tl) detector

4.1 Approach based on net areas

We first apply a similar method as previously, based on net area extraction, to the 92 keV (^{238}U) and 186 keV (^{235}U) gamma peaks, which are the most visible ones and are characteristic of the uranium contamination in the NaI(Tl) spectrum (see Figure 5). Note that they are absent in the background spectrum (see further Figure 9). The estimation of the net areas is however more complex than with the HPGe detector due to the NaI(Tl) poor energy resolution. Especially, the 92 keV peak overlaps with the 85, 87, and 90 keV X-rays (see Fig. 5 above with the HPGe detector vs. Fig. 7 below) due to both X-ray fluorescence of the lead shield and to internal conversion de-excitations. Daughter isotopes of the natural U and Th decay chains (see Fig. 1 from [1]) de-excite by ejecting internal conversion electrons, which are followed by the emission of Bi and Pb X-rays. For instance, lead X-rays can be emitted after the decay of ^{210}Tl into ^{210}Pb in the ^{238}U chain, with respective intensities of 3.8 % and 1.1 % for the 85.0 keV and 87.6 keV lead X-rays [2]. In the same ^{238}U chain, the decay of ^{214}Pb into ^{214}Bi leads to the emission of bismuth X-rays at 87.3 and 90.1 keV, with respective intensities of 3.6 % and 1.1 %. In the ^{232}Th chain, the decay of ^{212}Pb into ^{212}Bi gives birth to the same bismuth X-rays, but with intensities of 5.8 % and 1.8 %.

Therefore, we use two Gaussian curves for the fit shown in Figure 7 (contrary to the 186 keV peak fitted with a single Gaussian), which leads to significant variations on the 92 keV net area depending on the parameters of the fit (e.g. window size). By varying these parameters, we estimated this systematic uncertainty to 30 %. The contribution of the natural decay chain of ^{238}U at 92 keV and 186 keV (mainly due to ^{226}Ra for the latter) was extrapolated from the net area of the 609 keV peak emitted by ^{214}Bi (visible in further Fig. 8). This last is in equilibrium with ^{238}U and we use the $\frac{Eff_{MCNP}(92\text{ keV}) \times I_{\%}(92\text{ keV})}{Eff_{MCNP}(609\text{ keV}) \times I_{\%}(609\text{ keV})}$ and $\frac{Eff_{MCNP}(186\text{ keV}) \times I_{\%}(186\text{ keV})}{Eff_{MCNP}(609\text{ keV}) \times I_{\%}(609\text{ keV})}$ efficiency ratios calculated with MCNP for a uniform distribution multiplied by the emission intensity [2] of these natural gamma-ray emitters in the soil concrete. Then these extrapolated background contributions of 6.0 % and 6.2 % were subtracted from the respective 92 keV and 185 keV net areas.



28

29 Figure 7 : Gaussian 1 fit of the 92 keV gamma ray of ^{238}U contamination (green curve) and Gaussian 2 fit of the unresolved
30 85, 87 and 90 keV lead and bismuth X-rays (pink curve).

1 As in section 3, we calculate detection efficiencies for the NaI(Tl) detector with MCNP simulations using
2 the numerical model of Figure 4 and we estimate ^{238}U and ^{235}U surface activities with (1):

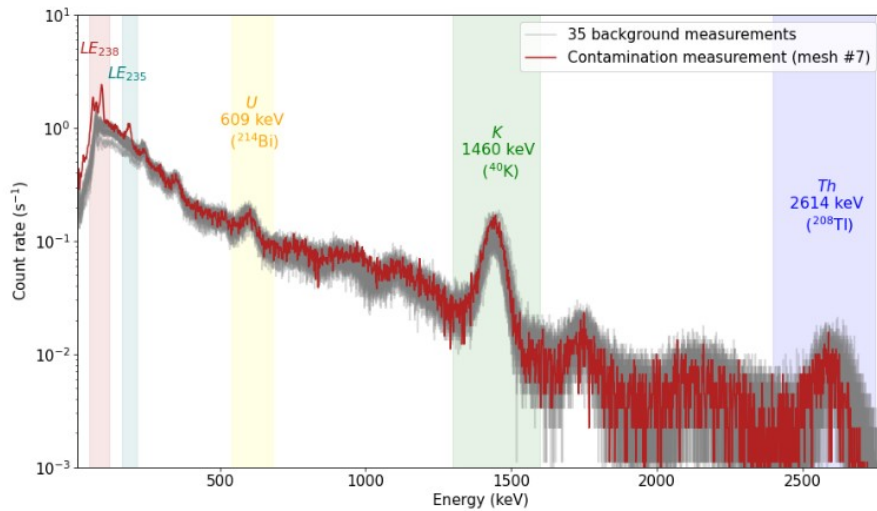
- 3 - $A_s(^{238}\text{U}) = (4.2 \pm 1.4) \text{ Bq.cm}^{-2}$,
- 4 - $A_s(^{235}\text{U}) = (0.24 \pm 0.05) \text{ Bq.cm}^{-2}$.

5 We note relative differences of + 26% and + 33%, respectively, with respect to HPGe measurement,
6 see Table 2.

7 The error budget in this case is similar to the one listed for the HPGe detector in previous section, but
8 with a larger uncertainty on net area extraction due to the lower resolution of the NaI(Tl) detector.
9 Therefore we estimate total relative uncertainties of about 30 % and 10 % on activities estimated with
10 the NaI(Tl) and HPGe detectors, respectively. The ^{238}U and ^{235}U activities measured with the NaI(Tl)
11 result in a uranium enrichment $\eta_U = (0.93 \pm 0.35) \%$ that is consistent at 1σ with the reference HPGe
12 value $\eta_U = (0.83 \pm 0.07) \%$. However, the extraction of the 63 and 92 keV net area characteristic of ^{238}U ,
13 in the NaI(Tl) spectrum, is only possible at low enrichment. Indeed, at higher enrichment levels, the
14 ^{238}U activity proportion drops and these peaks are no longer detectable. Therefore, we present in next
15 section a new method based on energy bands of the gamma spectrum that can be used in higher
16 enrichment plants.

17 4.2 A new method based on energy bands

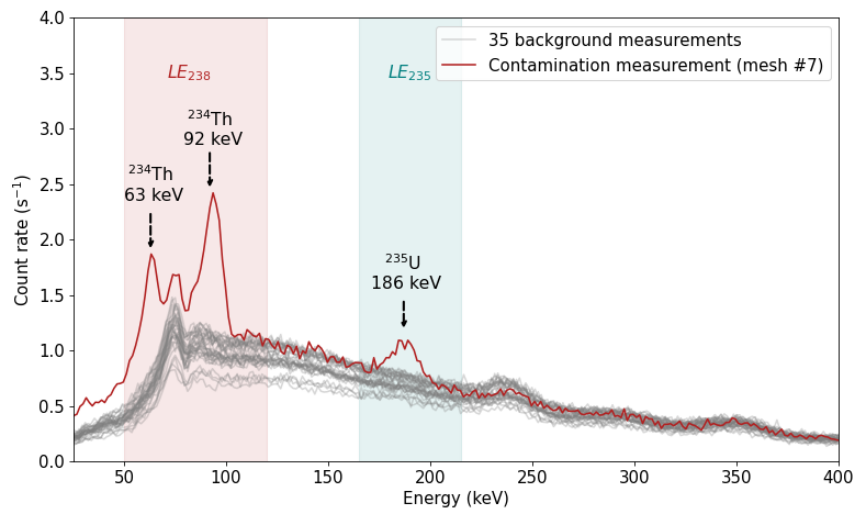
18 The following methods are covered by patent application FR2210553 “Method for the detection of
19 uranium contamination and estimation of $^{235}\text{U}/^{238}\text{U}$ enrichment level using low resolution gamma
20 spectrometry”. They use the number of counts in energy bands (see Figure 8), some of which contain
21 information on uranium contamination, especially at low energy. As the contamination signal in these
22 bands is very small compared to the background noise, and as the latter may vary depending on
23 concrete composition, we need a precise evaluation of the background in each measured spectrum.
24 The contamination signal is between 50 and 120 keV (“LE₂₃₈” band) including the main gamma rays
25 specific of ^{238}U , *i.e.* the 63.3 and 92 keV peaks of its direct daughter ^{234}Th . For ^{235}U , we define a “LE₂₃₅”
26 band from 165 to 215 keV, around its main 186 keV gamma ray. The proposed method to assess the
27 background in these bands exploits higher energy regions including well-known gamma rays of the
28 natural radioactivity present in concrete (uranium and thorium chains, ^{40}K [1]) and a regression model
29 to predict the corresponding low-energy background. Figure 8 shows 35 background spectra (in grey)
30 acquired on contamination-free areas at the UDG low, high, and very-high enrichment plants. For
31 comparison, the contamination spectrum is reported as well (in red). These background spectra have
32 an acquisition time of 900 s, except two longer acquisitions of 37 min and 2.5 h, respectively. Figure 8
33 also shows the selected energy bands, named “U”, “K” and “Th” according to the main background
34 peaks on which they are centered (609 keV for ^{238}U chain, 1460 keV peak for ^{40}K and 2614 keV for ^{232}Th
35 chain), and the two low-energy bands LE₂₃₈ and LE₂₃₅ mentioned above, used to characterize uranium
36 contamination.



1

2 *Figure 8 : Low Energy (LE) bands LE_{238} and LE_{235} including the ^{238}U and ^{235}U surface contamination signals, respectively, and*
 3 *U, K, Th natural background energy bands.*

4 We note the absence of 63.3, 92 and 186 keV peaks in background spectra, as highlighted in
 5 Figure 9 below.



6

7 *Figure 9 : Comparison at low energy of the contamination spectrum (including also the background) and of a background*
 8 *spectrum acquired at the Low Enrichment Plant.*

9 Only a peak around 75 keV is common to both spectra, due to both the fluorescence of the lead shield,
 10 and Bi or Pb rearrangement X-rays following the ejection of internal conversion electrons
 11 (de-excitation of daughter nuclei in the natural decay chains of U and Th). For instance, the decay of
 12 ^{210}Tl into ^{210}Pb in the ^{238}U chain, leads to the emission of 72.8 and 75.0 keV lead X-rays with intensities
 13 of 7.00 % and 11.0 %, respectively [2]. Likewise, the decay of ^{214}Pb into ^{214}Bi emits 74.8 and 77.1 keV
 14 bismuth X-rays, with respective intensities of 6.26 % and 10.5 %. In the ^{232}Th natural chain, the decay
 15 of ^{212}Pb into ^{212}Bi gives birth to the same bismuth X-rays, but with intensities of 10.0 % and 16.9 %.
 16 Our patent-pending approach is to predict the natural background counts inside the LE_{238} and LE_{235}
 17 bands using a simple linear regression model. The input data are the counts in the U, K and Th bands
 18 of Figure 8, and the regression uses the 35 background spectra, assuming that the counts in the two

1 low-energy regions of interest are a linear combination of the counts in the U, K and Th background
 2 regions:

3
$$LE_{238 \text{ or } 235} = a_U \times U + a_K \times K + a_{Th} \times Th \quad (3)$$

4 with:

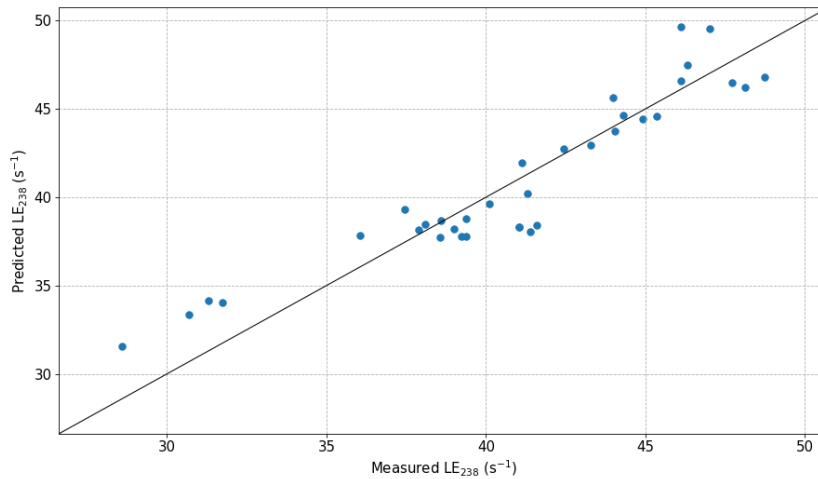
- 5 - $LE_{238 \text{ or } 235}$ the estimated background counts in the low energy regions, respectively from 50 to
- 6 120 keV and from 165 to 215 keV,
- 7 - U the experimental counts inside the uranium background region (540 to 680 keV),
- 8 - K the experimental counts inside the potassium background region (1300 to 1600 keV),
- 9 - Th the experimental counts inside the thorium background region (2400 to 3100 keV),
- 10 - a_U, a_K and a_{Th} the regression parameters.

11 The regression parameters are given in Table 3, Figure 10 and 11 show a comparison between
 12 predicted and measured (true) values of LE_{238} and LE_{235} , respectively.

13 *Table 3 : Regression parameter values for the prediction of count rates inside the LE_{238} and LE_{235} energy bands.*

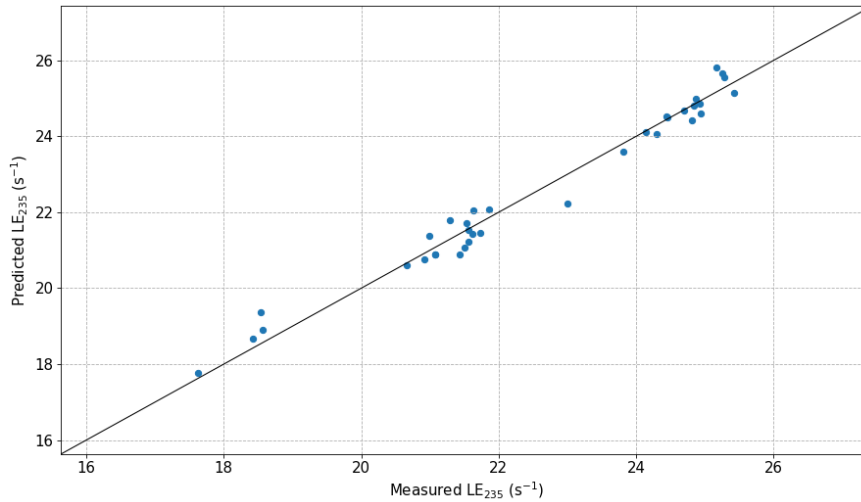
Parameter	LE_{238} model	LE_{235} model
a_U	2.48×10^0	1.89×10^0
a_K	1.62×10^0	-1.98×10^{-2}
a_{Th}	-3.11×10^0	2.90×10^{-2}

14



15

16 *Figure 10 : Predictions of the LE_{238} regression model as a function of measured values. The $Y=X$ black line is plotted for visual*
 17 *purposes.*



1

2 *Figure 11 : Predictions of the LE_{235} regression model as a function of measured values. The $Y=X$ line is plotted for visual*
 3 *purposes.*

4 The SMAPE (Symmetric Mean Absolute Percentage Error) associated with the LE_{238} and LE_{235} models
 5 are respectively 3.7 % and 1.2 %, showing that they correctly predict the background count rates in
 6 these energy bands. Table 4 gives the measured count rates of U, K and Th as well as predicted
 7 background count rates in LE_{238} and LE_{235} bands for the contamination spectrum measured in the
 8 middle of mesh #7 (see Figure 5 and Figure 8).

9 *Table 4 : Experimental count rates for U, K and Th energy bands and predicted background in LE_{238} and LE_{235} energy bands.*

Energy band	Count rate (s^{-1})	Uncertainty (s^{-1})
U	12.1	0.1
K	10.1	0.1
Th	0.86	0.03
LE_{238} (predicted background)	43.6	2.1
LE_{235} (predicted background)	22.6	0.4

10 Table 4 shows that a 15 min measurement over the contaminated area allows the prediction of
 11 background counts on the LE_{238} and LE_{235} bands with relative uncertainties of 4.7 % and 1.9 %
 12 respectively. Additionally, it is possible to reduce measurement times even further while keeping a low
 13 relative uncertainty. For example, applying these models to a 2 min contamination measurement
 14 would lead to only 5.1 % and 3.1 % relative uncertainties on predicted LE_{238} and LE_{235} background
 15 counts.

16 Finally, the predicted backgrounds of Table 4 are subtracted to the raw count rates of the low energy
 17 bands ($67.7 \pm 0.3 s^{-1}$ for LE_{238} and $27.8 \pm 0.2 s^{-1}$ for LE_{235}), leading to following net count rates
 18 $\tau_{LE_{238}} = 24.2 \pm 2.1 s^{-1}$ and $\tau_{LE_{235}} = 5.2 \pm 0.4 s^{-1}$. For the activity estimation, we use the LE_{238} band that
 19 presents a higher signal-to-noise ratio than LE_{235} . In higher enrichment plants, the LE_{235} energy band
 20 would be preferred. The net area analysis used before with (1) does not apply here with multiple
 21 gamma peaks in the LE_{238} energy band. Instead, the surface activity estimation requires a calibration
 22 coefficient (CC) representing the count rate per unit of surface activity (in $s^{-1} \cdot Bq^{-1} \cdot cm^2$ unit) of the
 23 contamination. CC is determined with MCNP and the model of Figure 4, considering a multiple gamma
 24 source according to the activity fractions of ^{238}U , ^{235}U and ^{234}U measured with the HPGe detector

1 (Table 2). The obtained calibration coefficient is $CC_{LE238} = 2.5 \pm 0.3 \text{ s}^{-1} \cdot \text{Bq}^{-1} \cdot \text{cm}^2$ and we calculate the
 2 total surface activity of uranium with (6).

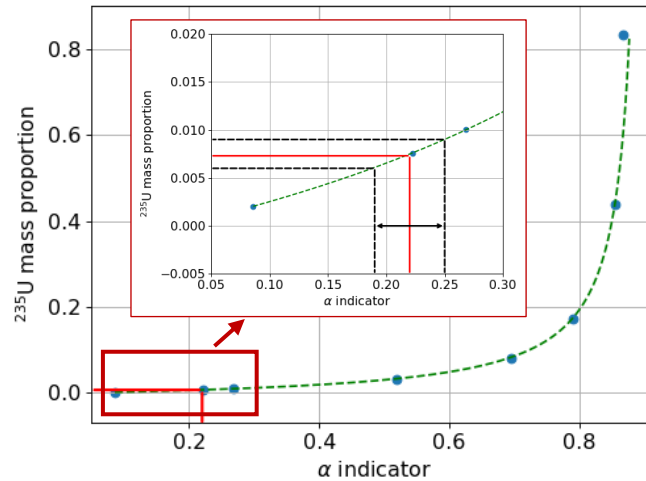
$$3 \quad A_s = \frac{\tau_{LE238}}{CC_{LE238}} = 9.8 \pm 1.4 \text{ Bq} \cdot \text{cm}^{-2} \quad (6)$$

4 This value is consistent with the HPGe measurement $A_s = (7.47 \pm 0.75) \text{ Bq} \cdot \text{cm}^{-2}$, but with a larger relative
 5 uncertainty (14 % vs. 10 %). Nonetheless, acquisition time was 65 h with the HPGe detector and
 6 15 min here with the NaI(Tl) one, and possibly even less as mentioned above
 7 (2 min). With our current NaI(Tl) setup, the Minimum Detectable Activity (MDA) in 15 min is
 8 $0.5 \text{ Bq} \cdot \text{cm}^{-2}$, which is close to the clearance level of $0.4 \text{ Bq} \cdot \text{cm}^{-2}$. Further setup optimizations, such as
 9 using an array of 3x3 NaI(Tl) detectors with the same individual dimensions 4"x4"x2", are planed to
 10 reach an MDA lower than this decommissioning threshold. It is however important to mention that
 11 this MDA only applies for the detection of low-enrichment contaminations, here 0.8 %. At higher
 12 enrichment, the MDA will be higher because the ^{238}U activity proportion decreases. In these cases, one
 13 can carry out the same type of analysis based on the LE_{235} band, which takes into account the 186 keV
 14 gamma emission from ^{235}U .

15 Regarding uranium enrichment, we use the " α " indicator defined in (7) as the ratio of the above net
 16 count rates LE_{235} and LE_{238} :

$$17 \quad \alpha_{EXP} = \frac{\tau_{LE\ 235}}{\tau_{LE\ 238}} = 0.22 \pm 0.03 \quad (7)$$

18 and using MCNP simulation we establish a calibration curve between enrichment and this indicator,
 19 see Figure 12.



20
 21 *Figure 12 : Calibration curve of ^{235}U enrichment (mass proportion) as a function of the measured α indicator.*

22 The measured value $\alpha_{EXP} = 0.23$ (red line) leads to an enrichment $\eta_U = (0.73 \pm 0.15) \%$ when taking into
 23 account the 13 % relative uncertainty on α_{EXP} (dashed black lines), which is consistent with that of the
 24 HPGe detector, $\eta_U = (0.83 \pm 0.07) \%$. Although less precise than HPGe, this NaI(Tl) characterization of
 25 the contamination enables a much faster estimation of its surface activity, with a practically sufficient
 26 uncertainty of 30 %, and offers the possibility to check the enrichment order of magnitude, within a
 27 few minutes of acquisition.

1 5 Conclusion

2 Measurements of an uranium contaminated area were carried out with HPGe and NaI(Tl) detectors at
3 the UDG gaseous diffusion enrichment plant of Pierrelatte, France. A reference HPGe measurement of
4 65 h gives a total surface activity (i.e. the sum of ^{234}U , ^{235}U and ^{238}U activities) of
5 $A_s = 7.47 \pm 0.75 \text{ Bq.cm}^{-2}$ and a uranium enrichment of $\eta_U = (0.83 \pm 0.07) \%$ in terms of ^{235}U mass
6 fraction, as expected for this low-enrichment plant.

7 In view to reduce measurement times, we also report a 15 min acquisition with a low-resolution NaI(Tl)
8 detector, on the same contaminated spot. First, the usual analysis based on net areas of the 92 keV
9 peak of ^{234}Th , direct daughter of ^{238}U , and 185 keV peak of ^{235}U leads to surface activities consistent
10 with HPGe results: $(4.2 \pm 1.4) \text{ Bq.cm}^{-2}$ vs. $(3.33 \pm 0.33) \text{ Bq.cm}^{-2}$ for ^{238}U with the NaI(Tl) and HPGe
11 detectors, respectively, and $(0.24 \pm 0.05) \text{ Bq.cm}^{-2}$ vs. $(0.18 \pm 0.02) \text{ Bq.cm}^{-2}$ for ^{235}U . The enrichment
12 estimated with this approach, $\eta_U = (0.93 \pm 0.35) \%$, is also consistent with HPGe. The largest
13 uncertainties stem from the difficulty to extract precise net areas due to the poor energy resolution of
14 NaI(Tl) compared to that of HPGe.

15 However, the 92 keV peak will be too weak in higher enrichment plants to allow for its net area
16 extraction with the NaI(Tl) detector. Therefore, we also report an innovative method based on energy
17 bands of the NaI(Tl) gamma spectrum at low energy, and on a multi-linear regression model to
18 estimate the natural background of concrete underlying the contamination. This alternative approach
19 leads to a total surface activity of $A_s = (9.8 \pm 1.4) \text{ Bq.cm}^{-2}$ and to an enrichment level of
20 $0.73 \pm 0.15 \%$. These different results show that it is possible to use NaI(Tl) detectors for a fast
21 assessment of the contamination activity and enrichment, within a few minutes, as the limiting factor
22 regarding uncertainty is not the current 15 min measurement time. In addition, the possibility of using
23 large area NaI(Tl) scintillators at a reasonable cost will allow scanning the wide UDG enrichment plants
24 (hundreds of thousands of squared meters) within practical times.

25 References

- 26 [1] F. Salvador *et al.*, "Gamma-ray spectroscopy for the characterization of uranium contamination
27 in nuclear decommissioning," *EPJ Web Conf.*, vol. 288, p. 07005, 2023, doi:
28 10.1051/epjconf/202328807005.
- 29 [2] M.-M. Bé, V. Christé, and C. Dulieu, "NUCLÉIDE-LARA - Bibliothèque des émissions alpha, X et
30 gamma," *Rapport CEA R-6201*.
- 31 [3] S. Philippe and A. Glaser, "Nuclear Archaeology for Gaseous Diffusion Enrichment Plants,"
32 *Science & Global Security*, vol. 22, no. 1, pp. 27–49, Jan. 2014, doi:
33 10.1080/08929882.2014.871881.
- 34 [4] S. Leblond, P. Fichet, R. Laumonier, S. Billon, P. Sardini, and K. Colas, "Development of a compact
35 alpha and beta camera for dismantlement applications," *J Radioanal Nucl Chem*, vol. 331, no. 2,
36 pp. 1075–1089, Feb. 2022, doi: 10.1007/s10967-021-08172-2.
- 37 [5] S. Leblond, P. Fichet, R. Laumonier, S. Billon, and P. Sardini, "MAUD Project - development of a
38 new portable detector for alpha and beta surface contamination imaging," 2018.
- 39 [6] Mirion Technologies, "Falcon 5000® Portable HPGe-Based Radionuclide Identifier." Accessed: Jul.
40 26, 2022. [Online]. Available: [https://mirion.s3.amazonaws.com/cms4_mirion/files/pdf/spec-](https://mirion.s3.amazonaws.com/cms4_mirion/files/pdf/spec-sheets/falcon-portable-hpge-based-identifier.pdf?1557257239)
41 [sheets/falcon-portable-hpge-based-identifier.pdf?1557257239](https://mirion.s3.amazonaws.com/cms4_mirion/files/pdf/spec-sheets/falcon-portable-hpge-based-identifier.pdf?1557257239)
- 42 [7] G. F. Knoll, *Radiation detection and measurement*, 3rd ed. New York: Wiley, 2000.
- 43 [8] Los Alamos National Laboratory, "Monte Carlo N-Particle (MCNP) Transport Code." [Online].
44 Available: <https://laws.lanl.gov/vhosts/mcnp.lanl.gov/index.shtml>

- 1 [9] D. Erb, "pybaselines: A Python library of algorithms for the baseline correction of experimental
- 2 data", doi: 10.5281/zenodo.7255880.
- 3 [10] K. Edwards, "Isotopic analysis of uranium in natural waters by alpha spectrometry," 1968. doi:
- 4 10.3133/wsp1696F.
- 5